

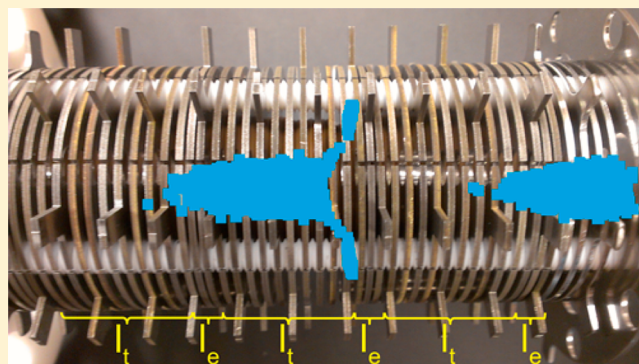
Gridless Overtone Mobility Spectrometry

Steven M. Zucker, Michael A. Ewing, and David E. Clemmer*

Department of Chemistry, Indiana University, Bloomington, Indiana 47405, United States

Supporting Information

ABSTRACT: A novel overtone mobility spectrometry (OMS) instrument utilizing a gridless elimination mechanism and cooperative radio frequency confinement is described. The gridless elimination region uses a set of mobility-discriminating radial electric fields that are designed so that the frequency of field application results in selective transmission and elimination of ions. To neutralize ions with mobilities that do not match the field application frequency, active elimination regions radially defocus ions toward the lens walls. Concomitantly, a lens-dependent radio frequency waveform is applied to the transmission regions of the drift tube resulting in radial confinement for mobility-matched ions. Compared with prior techniques, which use many grids for ion elimination, the new gridless configuration substantially reduces indiscriminate ion losses. A description of the apparatus and elimination process, including detailed simulations showing how ions are transmitted and eliminated is presented. A prototype 28 cm long OMS instrument is shown to have a resolving power of 20 and is capable of attomole detection limits of a model peptide (angiotensin I) spiked into a complex mixture (in this case peptides generated from digestion of β -casein with trypsin).



In recent years, ion mobility spectrometry (IMS) combined with mass spectrometry (MS) has been applied to a range of new fields, such as structural biology,^{1–4} proteomics,^{5,6} glycomics,^{7,8} and petroleomics.^{9,10} The complexity of samples that are encountered in these fields are spurring efforts to improve IMS-based separations, as well as the sensitivity of these techniques. To this end, a number of new mobility-based techniques are under development, including traveling wave ion mobility spectrometry,^{11–14} differential mobility analysis,^{15–17} field asymmetric waveform ion mobility spectrometry,^{18–24} and overtone mobility spectrometry (OMS).^{25–30}

Recently, our group has focused on the development of theory and instrumentation associated with OMS. In this approach a series of electrostatic gates are opened and closed at a defined frequency (called the field application frequency, and denoted f) such that only ions with mobilities that are resonant with the applied frequency traverse through the instrument and are detected. Ions with nonresonant mobilities are eliminated upon reaching a set of grids (which act as an elimination region) at times when the gate is closed to ion transmission. By scanning f , it is possible to obtain an OMS spectrum. It is intriguing that ions of a given mobility may traverse the device at a fundamental frequency (f_t), wherein matched-mobility ions move the length of one segment each time the phases switch, as well as at configuration-dependent multiples of f_t , hence the “overtone” designation in the name.

Having noted this, a complete understanding of how OMS instruments might be operated is somewhat complicated. Substantial insight can be gained by examining an expression for the resolving power, derived recently by Valentine et al.,²⁶

$$R_{\text{OMS}} = \frac{1}{1 - \left[1 - \frac{0.74}{\sqrt{n} R_{\text{IMS}}} \right] \left[\frac{mn - \left[\phi - 1 - \frac{l_t}{l_t + l_e} \right]}{mn} \right]} \quad (1)$$

In eq 1, n corresponds to the number of segments in the device and the terms l_t and l_e denote the lengths of the transmission and elimination regions, respectively. R_{IMS} is the resolving power of an equivalent IMS instrument with a length of one segment, described elsewhere.^{31–33} The term m designates configuration-dependent multiples of f_t where ions of a given mobility are also transmitted; ϕ is a variable that denotes the number of phases employed in the OMS device, as described previously.^{25,26} As examined in more detail previously, the value of 0.74 emerges from the assumption that all diffusion counteracts the field-directed separation of the ions. Replacing 0.74 with 0.00 yields the resolving power with no diffusion. This presents two extreme cases of diffusion with the former providing a lower bound and the latter an upper bound on the resolving power.²⁶ Because of this assumption, eq 1 underestimates the resolving power for a given configuration. Overall, from this expression we find that there are many interesting combinations of instrumental parameters which will lead to functional devices.³⁰

It is not as obvious from this expression that there are advantages and disadvantages to different configurations.³⁰ To

Received: May 24, 2013

Accepted: September 27, 2013

date, we have demonstrated advantages in sensitivity by working at low overtone numbers, incorporating high phase numbers, and by use of short devices.^{25–27} The resolving power can be improved by increasing the number of gating regions (i.e., increasing n ; to date the maximum value that has been examined is $n = 43$), by working in high overtone regions (the maximum value examined to date is $m = 37$), or by utilizing higher-order overtone series.^{27,28} Finally, we have recently demonstrated that instruments that combine multiple OMS separations (i.e., OMS–OMS)²⁹ are feasible. These devices have potential as extraordinarily high resolving power separations prior to MS. We note that in some ways OMS–OMS (as mobility separation and analysis method) is analogous to multiple quadrupole MS–MS methods (for m/z separation and analysis).

Although early proof-of-concept OMS devices appear promising, several factors still limit these methods. First, because of the use of mesh grids in gating regions we experience losses of ions that should be transmitted. Second, initial designs were constructed as large instruments (several meters in length); it would be of use to develop more compact instruments. Finally, as ions drift down the axis of the OMS instrument they expand radially because of diffusion. This limits the length of OMS instruments that can be developed. This paper describes a new instrument that aims to address all three of these limitations – a gridless 28 cm long design that utilizes radio frequency (RF) confinement down the axis of the instrument. The result is a highly efficient, compact device. Molecular simulations are used to better understand how ions are confined and eliminated in the new mechanism. The instrument is demonstrated by examining the model peptide substance P. Studies aimed at understanding the utility of this method for analyzing low-abundance components of complex mixtures are presented.

EXPERIMENTAL SECTION

Instrumentation. General aspects of experiment and theory associated with OMS are presented elsewhere;^{25–30} however, the geometry, length, and method of ion elimination are unique to this instrument and are discussed in detail here. Figure 1 shows a schematic diagram and photograph of the new gridless overtone mobility spectrometry instrument. For purposes of development, the OMS instrument was inserted into a home-built ion mobility spectrometry–mass spectrometry (IMS–IMS–IMS–MS) instrument that has been described previously³⁴ and is shown in Figure 1. This instrument simply serves as a platform and provides a convenient source, mass analyzer, detector and data acquisition system. To ensure that mobility separations of ions were conducted by the OMS device alone, the Tyndall shutters and source gate on the IMS–MS instrument³⁴ were not used, resulting in the drift tube operating as an ion transfer tube. In the manner described in our previous work,³⁴ the entire drift tube assembly was maintained at 2.72 ± 0.02 Torr Helium and operated at room temperature (300 K) for all of the experiments presented here.

As shown in Figure 1, the 28 cm long device was composed of 9 identical segments, each with an elimination region and a transmission region, with an additional elimination region to define the exit of the device. The transmission regions were composed of 10 concentric lenses, each with an inner diameter of 0.635 cm, an outer diameter of 5.08 cm, a thickness of 0.137 cm, and spaced by o-rings that were 0.137 cm thick when

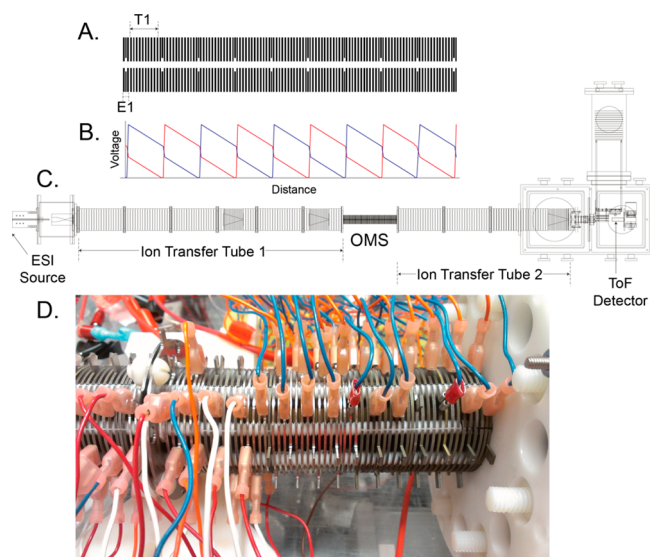


Figure 1. (A) The schematic diagram of the gridless OMS device. The OMS lens spacing and relative size can be seen with the first elimination (E1) and first transmission (T1) regions labeled. (B) Potentials as applied to the lenses to generate transmissive and eliminative fields are shown. The x -axis of parts A and B are aligned. (C) The schematic of the complete instrument; the gridless OMS device which has been coupled to our previously built IMS–MS instrument with an ESI source, three funnels within IMS drift tubes, used in this case as ion transfer tubes, and a time-of-flight mass analyzer. (D) A photograph of about half the OMS–MS instrument including the mounting region to ion transfer tube 2. The mounting plate is shown on the right as a white polyacetal plate while the colored wires for individual connections to lenses are shown surrounding the instrument.

compressed. The elimination regions were composed of 3 additional concentric lenses spaced with a compressed 0.058 cm thick o-ring. The first and last elimination rings were identical to the lenses in the transmission region; however, the center elimination lens had an inner diameter of 1.27 cm.

Potentials were applied to the lenses in order to generate OMS electric fields as shown in figure 1, similar to configurations used and described previously.^{25,26,35} A field of $9.8 \text{ V}\cdot\text{cm}^{-1}$ was used in transmission regions while a field of $31 \text{ V}\cdot\text{cm}^{-1}$ was applied to inactive (transmitting) elimination regions, the latter to improve signal due to the large relative length of the elimination region. An additional RF sine wave was applied to the lenses within each transmission region in order to radially confine the ions as they traveled down the axis of the drift tube. The 650 kHz, $75 \text{ V}_{\text{p-p}}$ sine wave applied to each lens was 180 degrees out of phase from adjacent lenses, as described previously.³⁶ The applied frequency and voltage were selected based on previously derived theory³⁷ and optimized to result in high transmission. In order to eliminate ions of mismatched mobility, the elimination regions defocused ions away from the middle of the drift tube, and therefore RF was not applied to the three lenses within the elimination region.

Resistors and capacitors used for voltage dividers and for coupling of RF, respectively, were laid out on a separate board and the appropriate nodes were connected to corresponding lenses. This minimized extraneous electrical short circuits generated while trying to fit a resistor between each pair of transmission lenses, a capacitor at each transmission lens, and connections from the waverdriver to 4 out of the 13 lenses in

each segment. Figure 1 gives a good sense of the scale of the instrument and the complexity in wiring such closely spaced lenses with the electronics commonly used previously.

Obtaining an OMS Distribution. To obtain an OMS distribution, mixtures of ions having different mobilities were electrosprayed (as described below) into ion transfer tube 1 (figure 1). A continuous beam of ions was transferred to the OMS region and OMS distributions were obtained by scanning the drift field application frequency as previously described.²⁵ As shown in Figure 1, voltages were applied at four discrete points on each segment to generate a positive potential from one transmission region through the next transmission region, pushing the ions toward the detector. In the first phase, the end of the second elimination region contained a repulsive field which prevented ions from drifting to the next segment and instead defocused them toward the lenses where they were neutralized. The applied voltages repeated every two segments, generating a sawtooth pattern similar to those in other OMS devices. A second sawtooth pattern, offset by one segment, was alternated with the first at the field application frequency. Ions that were not eliminated in the OMS segments subsequently drifted through ion transfer tube 2, passed through a series of optical focusing devices, and entered the home-built time-of-flight (ToF) mass spectrometer where they were separated by mass and detected. OMS distributions were obtained by scanning the field application frequency in increments (typically 50 Hz) from 1000 to 30000 Hz.

Instrument Simulation. Ion trajectory simulations were performed with a program written in-house and described previously.^{26–28,30,38} The software package SIMION (Scientific Instrument Services, Inc., Ringoes, NJ)³⁹ was used to generate electric fields from experimental lens geometries and applied voltages. A range of geometries were explored via simulations before settling upon the final geometry presented herein. For each time step of a simulation, changes in ion position were calculated from the sum of the electric-field directed motion and a random diffusive motion obtained from the appropriate Gaussian distribution. In these simulations, 0.1 μ s time steps were used. When optimized for an effective elimination mechanism, the geometry and voltages led to indiscriminate radial elimination of many of the ions that were within the stable packet region at all times.³⁰ To minimize these indiscriminate radial losses, a lens-dependent RF waveform was applied to the transmission regions, leading to increased ion transmission without sacrificing the elimination of mobility-mismatched ions.

Sample Preparation and Electrospray Conditions. Substance P acetate ($\geq 95\%$ purity), angiotensin I (human, $\geq 90\%$ purity), and β -casein (bovine, $\geq 98\%$ purity) were purchased from Sigma-Aldrich (St. Louis, MO) and used without further purification. Substance P (50 μ g·mL⁻¹) and angiotensin I (concentrations from 100 pg·mL⁻¹ to 50 μ g·mL⁻¹) were prepared in solutions of water/acetonitrile/acetic acid (49/49/2 by volume). Tryptic digestion was performed as described previously⁴⁰ and the resulting peptides were dissolved in a solution of 49/49/2 water/acetonitrile/acetic acid (50 μ g·mL⁻¹). All samples were electrosprayed using a pulled-tip capillary at a flow rate of 18 μ L·hour⁻¹ using a syringe pump (KD Scientific, Holliston, MA). The solution in the capillary tip was biased at 2200 V above the potential applied to the instrument entrance aperture to provide electrosprayed ions.

RESULTS AND DISCUSSION

Radial Ion Elimination Mechanism. Previous OMS devices imposed significant ion losses because of the grids at the beginning and end of each elimination region.²⁵ For example, in our earlier paper we used 48 grids, each having 90% optical transmittance, which results in the transmission of only approximately 0.6% of a beam. In order to increase the transmission of matched-mobility ions, we have removed these grids, making it feasible to extend the instrument to higher numbers of segments and thereby achieve a higher resolving power. To replace the grids, it is necessary to understand their contributions to ion motion in OMS. In the previous elimination mechanism, ions drifted toward, and were neutralized on, grids in active elimination regions. With the removal of grids from the instrument, the conducting surface at which the ions were neutralized was also removed, requiring that ions be radially defocused from the primary transmitting axis of the instrument in order for neutralization to occur on lenses. Simulations demonstrated that elimination of ions of mismatched mobilities was less efficient for an instrument with a geometry identical to previous OMS instruments but without grids. Additionally, simulations demonstrated that the inclusion of a third lens in the elimination region enabled more efficient elimination. The use of a third lens to shape the elimination field results in perturbation of the fields within the transmission region. This perturbation reduces the size of the transmission region, thus eliminating a significant portion of mobility-matched ions and reducing the maximum obtainable overtone.³⁰ A compromise design in which we increased the inner diameter of the middle elimination lens and used shorter distances between lenses was used to minimize this perturbation.

On Axis RF Confinement for Enhancing Transmission. In the previous OMS device, an ion funnel was implemented after approximately a meter of drift tube.²⁵ This funnel radially focused the ions toward the center axis of the drift tube, reducing dispersive losses due to random diffusion.³⁸ In our new design the drift region inner diameter is smaller; thus, to avoid ion losses we have incorporated RF confinement along the entirety of the OMS instrument (with the exception of elimination regions). Figure 2 shows snapshots of the simulated instrument operated at the field application frequency corresponding to the $m = 3$ peak of the doubly charged substance P ions ($K_0 = 3.41 \text{ cm}^2 \cdot \text{V}^{-1} \cdot \text{s}^{-1}$).⁴² Simulations of the trajectories of doubly protonated substance P and triply protonated Substance P ($K_0 = 4.44 \text{ cm}^2 \cdot \text{V}^{-1} \cdot \text{s}^{-1}$),³⁵ shown in figure 2, demonstrate that radial confinement in transmission regions does not preclude the developed radial elimination mechanism. Triply protonated substance P ions are not matched to the field application frequency and are rapidly eliminated as the simulation progresses. The motion of ion packets observed in Figure 2 confirms that our description of ion motion is correct and provides a frame of reference for applying the previously derived mathematical description to the current instrument.^{26,28,30} Without the applied RF confinement fields, the ions diffused out toward the lenses and were eliminated indiscriminately. Figure S1 shows a 3- to 4-fold increase in ion signal through the drift tube at $3f_f$ with RF as compared to without RF. As mentioned below, the realized experimental improvement is substantially larger.

RF confinement in ion funnels has been previously demonstrated to result in mass bias as has been described in

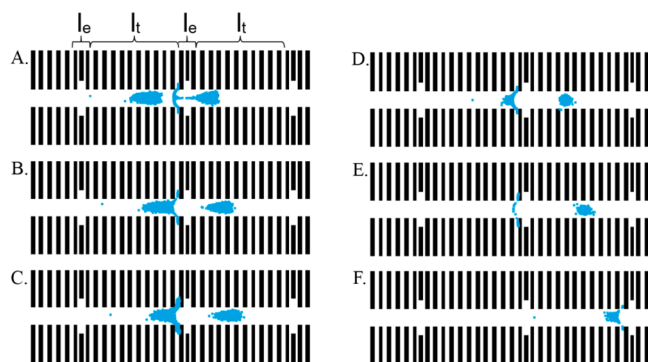


Figure 2. Snapshots of simulated substance P ions traversing the OMS system. Two of the elimination and transmission regions have been labeled with l_e and l_t , respectively. The left column (A, B, and C) are of doubly charged ions and the right column (D, E, and F) are the more elongated conformation of the triply charged peptide. Snapshots A and D were taken at $1425 \mu\text{s}$, B and E were at $1575 \mu\text{s}$, and C and F were taken at $1725 \mu\text{s}$ after the simulation began. In the presence of confining RF, $[M + 2H]^{2+}$ ions traversed the drift tube in two stable transmitting packets while the elimination of mobility-mismatched $[M + 3H]^{3+}$ ions was observed, consistent with previous descriptions of OMS.

depth elsewhere.³⁷ While the frequency and amplitude of the applied RF could alter the signal intensity as described previously,³⁷ no large mass bias was noticed in the current instrument. Due in part to the confounding effects of mass discrimination from the RF applied to the ion funnels in both ion transfer tubes, a detailed study was not performed. As we continue to develop this technique, we are investigating the effect of RF amplitude and frequency on the resolving power and signal intensity for different instruments and configurations.

Demonstration of OMS Instrument: Analysis of Substance P. Figure 3 shows typical OMS distributions obtained upon electrospraying substance P. Under the ESI conditions that are employed, we produce primarily the +2 and +3 charge states. Because the data are collected after MS analysis it is straightforward for us to plot ion intensities as a

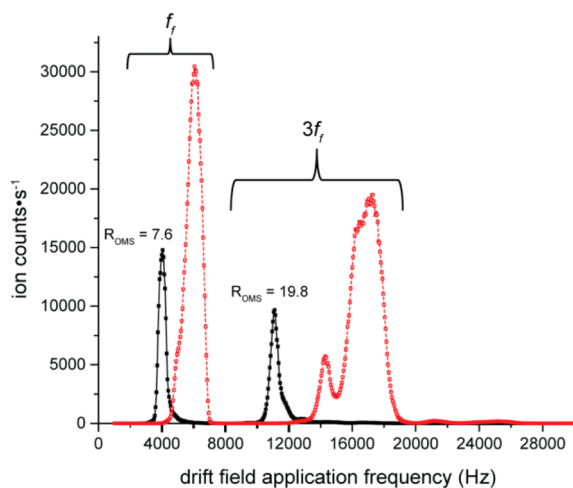


Figure 3. Mobility distributions of the +2 and +3 charge states of substance P in black and red respectively. Overtone regions and the resolving power of the peaks from the doubly protonated species are labeled.

function of drift field application frequency for each of the two ions. As expected, these distributions fall into two regions: one at the fundamental frequency and the second at three times that frequency ($3f_f$).^{26,30} We have previously developed an analytical expression for the maximum observable overtone of a given geometry,³⁰

$$m_{\max} = \frac{(l_e + l_t)}{l_e} \quad (2)$$

We calculate that $m_{\max} = 5.1$ from fields generated by SIMION without RF; however, the $m = 5$ peak was not observed experimentally for either charge state of substance P. This is not surprising as the signal becomes very small as m approaches m_{\max} .³⁰ Overtone peaks have approximately the same width as the peak at f_f ^{25,28} but are observed at higher frequencies, resulting in higher resolving powers and better separations in the $m = 3$ region than in the f_f region. This increase in resolving power also yields a better separation of the peaks associated with the doubly and triply charged ions in the $m = 3$ region relative to the f_f region. We also note that at $m = 3$, the two known conformers of the $[M + 3H]^{3+}$ species are resolved with peaks at 14300 and 17300 Hz; these conformations are not resolved at f_f .

Because the +2 charge state has only one major feature in the $m = 3$ region (at 11100 Hz), we use it as a benchmark of resolving power. In the present measurement, we find $R_{\text{OMS}} = 7.6$ for the peak associated with the substance P $[M + 2H]^{2+}$ ion. The resolving power increases to $R_{\text{OMS}} = 19.8$ when measured as the $3f_f$ peak. This corresponds to an increase of a factor of ~ 2.6 , better than the increase of 1.8 expected from eq 1 in the “worst-case” assumption about diffusion, and slightly worse than the value of 3.0 expected assuming no diffusion.

In prior work we have argued that an advantage of OMS measurements is that collision cross sections (Ω) can be determined directly from eq 3.²⁶

$$\Omega = \frac{(18\pi)^{1/2}}{16} \times \frac{ze}{(k_b T)^{1/2}} \times \left[\frac{1}{m_1} + \frac{1}{m_b} \right]^{1/2} \times \frac{E[\phi(h-1) + 1]}{f(l_e + l_t)} \times \frac{760}{P} \times \frac{T}{273.2} \times \frac{1}{N} \quad (3)$$

In eq 3, z is the charge of the ion (known experimentally from the MS measurement), e is the elementary charge, k_b is Boltzmann’s constant, T is the temperature, m_1 is the mass of the ion, m_b is the mass of the buffer gas, E is the electric field, h is the index to relate OMS phase and harmonic frequency,²⁶ P is the pressure, and N is the neutral number density under STP conditions. For systems such as small oligosaccharides, peptides, and the protein ubiquitin (which have been studied extensively)^{27,41} we find that OMS measurements (obtained using devices in which transmission and elimination regions are defined by grids) agree with previously reported IMS values to within 1% relative uncertainty.²⁷

Because the field in the present OMS device is not uniform (because of the step in field that is employed, as well as the gridless design) it is important to assess the ability of this device to accurately determine cross sections. To make this comparison, we used an average field to determine collision cross sections. We are immediately struck by the fact that the positions of peaks for the +2 charge state of substance P yield different values when determined from the f_f and $3f_f$ peaks, Ω_{f_f}

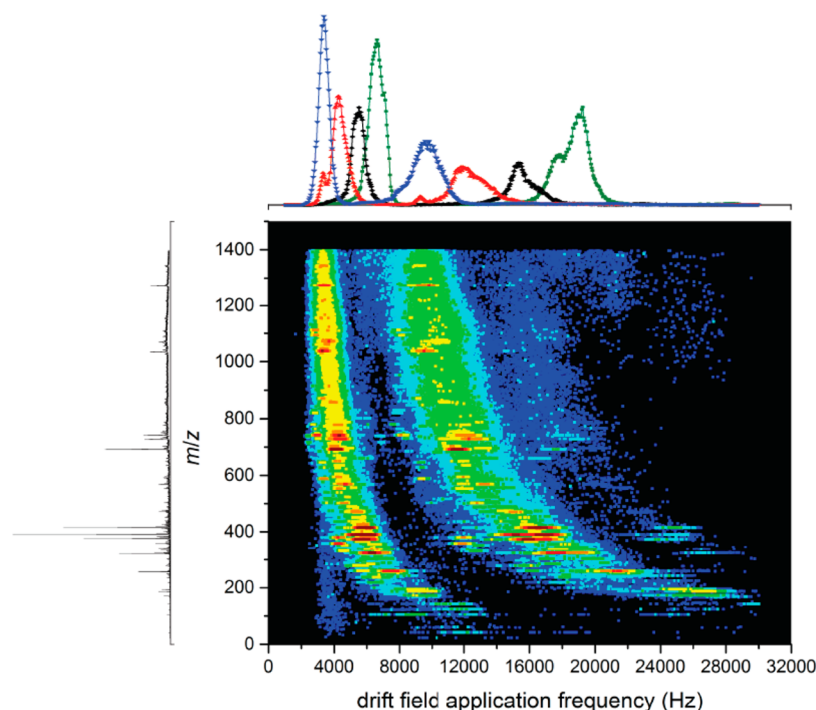


Figure 4. Two-dimensional frequency and m/z plot for the β -casein and angiotensin I solution used for the sensitivity scans is displayed in a false color plot. Above the nested plot is the extracted frequency distributions for each of the four observed charge states of angiotensin I across all isotopes. The singly ($1297 m/z$), doubly ($649 m/z$), triply ($433 m/z$), and quadruply ($325 m/z$) protonated angiotensin I are shown in blue, red, black, and green, respectively. The compressed mass spectrum, equivalent to the mass spectrum obtained if the solution was sprayed on a traditional mass spectrometer, is displayed on the left side of the figure.

= 283 \AA^2 and $\Omega_{3f_f} = 312 \text{ \AA}^2$. The most accurate cross section determined by IMS for this ion is $\Omega = 314 \text{ \AA}^2$,⁴² consistent with the $\Omega_{3f_f} = 312 \text{ \AA}^2$ value. For the dominant peak of the +3 charge state in the f_f region, a peak that contains overlapping conformations, we determine $\Omega_{f_f} = 284 \text{ \AA}^2$, substantially lower than the values of $\Omega_{3f_f} = 298$ and 362 \AA^2 , respectively, that we obtain from the peaks in the $m = 3$ region (in which multiple conformers are resolved). This ion has also been examined previously by IMS³⁵ and the measured cross sections for the compact and elongated conformers are 320 and 362 \AA^2 , respectively.

Clearly both peaks at the fundamental frequency appear to be significantly lower in cross section when compared to IMS measurements. This relative error is large ($\sim 10\%$). We attribute this to the nonuniform fields used to increase signal as well as the loss in field definition upon removing grids. As we develop higher-resolving power systems we are working toward determining accurate collision cross sections without the use of calibrations; however, this work is at an early stage and is not described in detail here. One approach is to utilize our simulation software. One could envision an algorithm that iteratively generates OMS distributions in order to search for the mobility that matches the experimentally obtained distribution. We anticipate that this should allow for more accurate cross sections to be calculated from gridless OMS measurements.

Assessment of Instrument Sensitivity. Finally, it is interesting to investigate the sensitivity of the new instrument. As we have stated, relative to prior instruments, sensitivity should be increased by the elimination of grids as well as by the incorporation of RF confinement. One assessment of sensitivity

is to determine the detection limits for a known analyte. In the case presented here we have doped the analyte into a complex mixture. For illustration purposes we examine the angiotensin I peptide in a mixture of peptides obtained from a tryptic digestion of β -casein. Although the simulations shown in Supporting Information Figure S1 showed a 3- to 4-fold decrease in signal without the inclusion of RF, no signal was observed experimentally in the absence of RF confinement.

Figure 4 shows a two-dimensional field application frequency versus m/z plot for equal concentrations of angiotensin I and β -casein digest. Similar to the substance P spectrum, the f_f and $3f_f$ peaks were observed for all charge states of angiotensin I; however, because of smaller diffusive losses for the higher charge states, the $5f_f$ peaks were also observed for the $[M + 3H]^{3+}$ and $[M + 4H]^{4+}$ species. The detection limits that we find for this system are remarkably low. For example, when 20 attomoles of angiotensin I were injected into the instrument at a field application frequency of 15300 Hz, the frequency corresponding to the $3f_f$ peak of the $[M + 3H]^{3+}$ ion, the signal-to-noise ratio at $433.2 m/z$ was found to be ~ 5 after background subtraction.

CONCLUSIONS

A new overtone mobility spectrometry instrument and accompanying gridless elimination mechanism has been described. This instrument has achieved a resolving power of 20 for substance P at a length of only 28 cm. RF confinement within transmission regions was utilized to significantly improve signal. Overall, the lens geometry and applied potentials create radially focusing transmission regions and radially defocusing elimination regions. We note that at this point, unlike the OMS designs that utilized grids (and uniform drift fields) the present

geometry has limited utility as a means of directly determining cross sections. Efforts are underway to address this limitation. The constructed instrument detected 20 attomoles of angiotensin I doped into a Tryptic digest of β -casein at a signal-to-noise ratio of 5.

■ ASSOCIATED CONTENT

● Supporting Information

Additional material as described in the text. This material is available free of charge via the Internet at <http://pubs.acs.org>.

■ AUTHOR INFORMATION

Corresponding Author

*E-mail: clemmer@indiana.edu.

Notes

The authors declare no competing financial interest.

■ ACKNOWLEDGMENTS

The authors acknowledge partial support of this work provided by grants from the Analytical Node of the METACyt initiative funded by a grant from the Lilly Endowment and by the NIH (1RC1GM090797-01). We are also grateful for the support of the Indiana University Mechanical and Electrical Instrumentation Services facilities and thank Rebecca S. Glaskin and Stephen J. Valentine for their helpful discussion and insight throughout this work.

■ REFERENCES

- (1) Ruotolo, B. T.; Verbeck, G. F.; Thomson, L. M.; Gillig, K. J.; Russell, D. H. *J. Am. Chem. Soc.* **2002**, *124*, 4214–4215.
- (2) Uetrecht, C.; Barbu, I. M.; Shoemaker, G. K.; Duijn, E. V.; Heck, A. J. R. *Nat. Chem.* **2010**, *3*, 126–132.
- (3) Counterman, A. E.; Clemmer, D. E. *J. Phys. Chem. B* **2003**, *107*, 2111–2117.
- (4) Hudgins, R. R.; Ratner, M. A.; Jarrold, M. F. *J. Am. Chem. Soc.* **1998**, *120*, 12974–12975.
- (5) Valentine, S. J.; Liu, X.; Plasencia, M. D.; Hilderbrand, A. E.; Kurulugama, R. T.; Koeniger, S. L.; Clemmer, D. E. *Expert Rev. Proteom.* **2005**, *2*, 553–565.
- (6) McLean, J. A.; Ruotolo, B. T.; Gillig, K. J.; Russell, D. H. *Int. J. Mass Spectrom.* **2005**, *240*, 301–315.
- (7) Isailovic, D.; Kurulugama, R. T.; Plasencia, M. D.; Stokes, S. T.; Kyselova, Z.; Goldman, R.; Mechref, Y.; Novotny, M. V.; Clemmer, D. E. *J. Proteome Res.* **2008**, *7*, 1109–1117.
- (8) Williams, J. P.; Grabenauer, M.; Holland, R. J.; Carpenter, C. J.; Wormald, M. R.; Giles, K.; Harvey, D. J.; Bateman, R. H.; Scrivens, J. H.; Bowers, M. T. *Int. J. Mass Spectrom.* **2010**, *298*, 119–127.
- (9) Li, Z.; Valentine, S. J.; Clemmer, D. E. *J. Am. Soc. Mass Spectrom.* **2011**, *22*, 817–827.
- (10) Becker, C.; Fernandez-Lima, F. A.; Russell, D. H. *Spectroscopy*. **2009**, *24*, 38–42.
- (11) Giles, K.; Pringle, S. D.; Worthington, K. R.; Little, D.; Wildgoose, J. L.; Bateman, R. H. *Rapid Commun. Mass Spectrom.* **2004**, *18*, 2401–2414.
- (12) Pringle, S. D.; Giles, K.; Wildgoose, J. L.; Williams, J. P.; Slade, S. E.; Thalassinou, K.; Bateman, R. H.; Bowers, M. T.; Scrivens, J. H. *Int. J. Mass Spectrom.* **2007**, *261*, 1–12.
- (13) Shvartsburg, A. A.; Smith, R. D. *Anal. Chem.* **2008**, *80*, 9689–9699.
- (14) Giles, K.; Williams, J. P.; Campuzano, I. *Rapid Commun. Mass Spectrom.* **2011**, *25*, 1559–1566.
- (15) Rosell-Llompart, J.; Loscertales, I. G.; Bingham, D.; Fernández de la Mora, J. *J. Aerosol. Sci.* **1996**, *27*, 695–719.
- (16) Labowsky, M.; Fernández de la Mora, J. *J. Aerosol. Sci.* **2006**, *37*, 340–362.
- (17) McMurry, P. H. *Atmos. Environ.* **2000**, *34*, 1959–1999.
- (18) Purves, R. W.; Guevremont, R.; Day, S.; Pipich, C. W.; Matyjaszcayk, M. S. *Rev. Sci. Instrum.* **1998**, *69*, 4094–4105.
- (19) Purves, R. W.; Guevremont, R. *Anal. Chem.* **1999**, *71*, 2346–2357.
- (20) Eiceman, G. A.; Tadjikov, B.; Krylov, E.; Nazarov, E. G.; Miller, R. A.; Westbrook, J.; Funk, P. J. *Chromatogr. A* **2001**, *917*, 205–217.
- (21) Shvartsburg, A. A.; Tang, K.; Smith, R. D. *J. Am. Soc. Mass Spectrom.* **2004**, *15*, 1487–1498.
- (22) Venne, K.; Bonneil, E.; Eng, K.; Thibault, P. *Anal. Chem.* **2005**, *77*, 2176–2186.
- (23) Shvartsburg, A. A.; Li, F.; Tang, K.; Smith, R. D. *Anal. Chem.* **2006**, *78*, 3706–3714.
- (24) Shvartsburg, A. A.; Mashkevich, S. V.; Smith, R. D. *J. Phys. Chem. A* **2006**, *110*, 2663–2673.
- (25) Kurulugama, R. T.; Nachtigall, F. M.; Lee, S.; Valentine, S. J.; Clemmer, D. E. *J. Am. Soc. Mass Spectrom.* **2009**, *20*, 729–737.
- (26) Valentine, S. J.; Stokes, S. T.; Kurulugama, R. T.; Nachtigall, F. M.; Clemmer, D. E. *J. Am. Soc. Mass Spectrom.* **2009**, *20*, 738–750.
- (27) Lee, S.; Ewing, M. A.; Nachtigall, F. M.; Kurulugama, R. T.; Valentine, S. J.; Clemmer, D. E. *J. Phys. Chem. B* **2010**, *114*, 12406–12415.
- (28) Valentine, S. J.; Kurulugama, R. T.; Clemmer, D. E. *J. Am. Soc. Mass Spectrom.* **2011**, *22*, 804–816.
- (29) Kurulugama, R. T.; Nachtigall, F. M.; Valentine, S. J.; Clemmer, D. E. *J. Am. Soc. Mass Spectrom.* **2011**, *22*, 2049–2060.
- (30) Ewing, M. A.; Zucker, S. M.; Valentine, S. J.; Clemmer, D. E. *J. Am. Soc. Mass Spectrom.* **2013**, *24*, 615–621.
- (31) Mason, E. A.; McDaniel, E. W. *Transport Properties of Ions in Gases*; Wiley: New York, 1988; pp 137–224.
- (32) Kemper, P. R.; Bowers, M. T. *J. Phys. Chem.* **1991**, *95*, 5134–5146.
- (33) Revercomb, H. E.; Mason, E. A. *Anal. Chem.* **1975**, *47*, 970–983.
- (34) Merenbloom, S. I.; Koeniger, S. L.; Valentine, S. J.; Plasencia, M. D.; Clemmer, D. E. *Anal. Chem.* **2006**, *78*, 2802–2809.
- (35) Merenbloom, S. I.; Glaskin, R. S.; Henson, Z. B.; Clemmer, D. E. *Anal. Chem.* **2009**, *81*, 1482–1487.
- (36) Julian, R. R.; Mabbett, S. R.; Jarrold, M. F. *J. Am. Soc. Mass Spectrom.* **2005**, *16*, 1708–1712.
- (37) Shaffer, S. A.; Tang, K.; Anderson, G. A.; Prior, D. C.; Udseth, H. R.; Smith, R. D. *Rapid Commun. Mass Spectrom.* **1997**, *11*, 1813–1817.
- (38) Koeniger, S. L.; Merenbloom, S. I.; Valentine, S. J.; Jarrold, M. F.; Udseth, H. R.; Smith, R. D.; Clemmer, D. E. *Anal. Chem.* **2006**, *78*, 4161–4174.
- (39) SIMION, version 8.0; Scientific Instrument Services, Inc.: Ringoes, NJ, 2006; www.simion.com.
- (40) Dilger, J. M.; Valentine, S. J.; Glover, M. S.; Ewing, M. A.; Clemmer, D. E. *Int. J. Mass Spectrom.* **2012**, *330–332*, 35–45.
- (41) Shi, H.; Gu, L.; Clemmer, D. E.; Robinson, R. A. S. *J. Phys. Chem. B* **2013**, *117*, 164–173.
- (42) Myung, S.; Lee, Y. J.; Moon, M. H.; Taraszka, J.; Sowell, R.; Koeniger, S.; Hildenbrand, A. E.; Valentine, S. J.; Cherbas, L.; Cherbas, P.; Kaufmann, T. C.; Miller, D. F.; Mechref, Y.; Novotny, M. V.; Ewing, M. A.; Clemmer, D. E. *Anal. Chem.* **2003**, *75*, 5137–5145.